

8. L. Prockter *et al.*, *Icarus* **155**, 75 (2002).
9. T. Michikami, K. Moriguchi, R. Nakamura, *36th Lunar Planet. Sci. Conf.*, abstr. 1729 (2005).
10. The slope of the bulk population would be somewhat steeper (0.2 to 0.3) than that of the surface population. See (26).
11. P. C. Thomas, J. Veveřka, M. S. Robinson, S. Murchie, *Nature* **413**, 394 (2001).
12. P. C. Thomas *et al.*, *J. Geophys. Res.* **105**, 15091 (2000).
13. M. J. Cintala, J. B. Garvin, S. J. Wetzel, *Proc. Lunar Planet. Sci. Conf.* **13**, 100 (1982).
14. J. E. Richardson, E. James, H. J. Melosh, R. J. Greenberg, D. P. O'Brien, *Icarus* **179**, 325 (2005).
15. C. R. Chapman *et al.*, *Icarus* **155**, 104 (2002).
16. S. Murchie *et al.*, *Icarus* **155**, 145 (2002).
17. P. Helfenstein *et al.*, *Icarus* **120**, 48 (1996).
18. J. Veveřka *et al.*, *Icarus* **120**, 66 (1996).
19. P. Helfenstein *et al.*, *Icarus* **107**, 37 (1994).
20. C. R. Chapman, *Meteorit. Planet. Sci.* **31**, 699 (1996).
21. S. Sasaki, K. Nakamura, Y. Hamabe, E. Kurahashi, T. Hiroi, *Nature* **410**, 555 (2001).
22. T. Hiroi, S. Sasaki, *Meteorit. Planet. Sci.* **36**, 1587 (2001).
23. B. E. Clark, B. Hapke, C. Pieters, D. Britt, in *Asteroids III*, W. Bottke *et al.*, Eds. (Univ. of Arizona Press, Tucson, 2002), pp. 585–599.
24. T. Hiroi, C. M. Pieters, H. Takeda, *Meteoritics* **29**, 394 (1994).
25. Gravitational sliding of regolith materials with different brightnesses was also observed on Eros. See (27).
26. W. K. Hartmann, *Icarus* **10**, 201 (1969).
27. P. C. Thomas *et al.*, *Icarus* **155**, 18 (2002).
28. We thank the mission operation and spacecraft team of the Hayabusa project at ISAS/JAXA for their efforts that led to Hayabusa being the first Japanese spacecraft to rendezvous with and land on the asteroid. This research was supported by ISAS/JAXA, NASA, Kobe University through "The 21st Century Center of Excellence Program of the Origin and Evolution of Planetary Systems," and the University of Aizu.

2 February 2006; accepted 20 April 2006
10.1126/science.1125722

REPORT

Mass and Local Topography Measurements of Itokawa by Hayabusa

Shinsuke Abe,^{1*} Tadashi Mukai,¹ Naru Hirata,^{1,3} Olivier S. Barnouin-Jha,² Andrew F. Cheng,² Hirohide Demura,³ Robert W. Gaskell,⁴ Tatsuaki Hashimoto,⁵ Kensuke Hiraoka,¹ Takayuki Honda,¹ Takashi Kubota,⁵ Masatoshi Matsuoka,⁶ Takahide Mizuno,⁵ Ryosuke Nakamura,⁷ Daniel J. Scheeres,⁸ Makoto Yoshikawa⁵

The ranging instrument aboard the Hayabusa spacecraft measured the surface topography of asteroid 25143 Itokawa and its mass. A typical rough area is similar in roughness to debris located on the interior wall of a large crater on asteroid 433 Eros, which suggests a surface structure on Itokawa similar to crater ejecta on Eros. The mass of Itokawa was estimated as $(3.58 \pm 0.18) \times 10^{10}$ kilograms, implying a bulk density of (1.95 ± 0.14) grams per cubic centimeter for a volume of $(1.84 \pm 0.09) \times 10^7$ cubic meters and a bulk porosity of $\sim 40\%$, which is similar to that of angular sands, when assuming an LL (low iron chondritic) meteorite composition. Combined with surface observations, these data indicate that Itokawa is the first subkilometer-sized small asteroid showing a rubble-pile body rather than a solid monolithic asteroid.

The light detection and ranging instrument (LIDAR) aboard the Hayabusa spacecraft, described in (1–4), provided information on the shape, surface topography, and mass of the near-Earth asteroid 25143 Itokawa. The LIDAR measures distance by determining the time of flight for laser light to travel from the spacecraft to the asteroid and return. The stop time measured by the LIDAR is obtained by filtering a pulse received from the surface and measuring its time of peak intensity. In this manner, the LIDAR averages the topography within the LIDAR footprint on the surface of the asteroid, which approximates 5 by 12 m at a 7-km altitude for normal incidence. It was found that this pulse-detection technique permits identifying features smaller than the LIDAR footprint.

The LIDAR operated from September 10, 2005, at a distance of 49 km from the target, through November 25; a total of 4,107,104 shots were fired, and 1,665,548 returns were detected. The numbers of returns reduced significantly after October 2 when spacecraft pointing was less accurate because of failures in two of the three on-board reaction wheels.

When the spacecraft arrived at Itokawa, we used two methods to confirm the accuracy of LIDAR ranging obtained from ground calibration of the LIDAR instrument (3) (± 1 m from a distance of 50 m and ± 10 m from 50 km). In one approach, the size of the spacecraft shadow that was cast on the asteroid surface at the center of opposition point in a navigation image equaled that expected given the LIDAR-measured range measured by the spacecraft. In another approach, the height of the largest boulder on Itokawa, namely Yoshinodai, was found to be ~ 20 m when using independent measurements obtained from the LIDAR and the narrow angle imager [Asteroid Multiband Imaging Camera (AMICA)].

The LIDAR beamwidth is 0.04° by 0.097° , and the boresight is coaligned with that of the near-infrared spectrometer (NIRS) with its 0.1° by 0.1° field of view. The NIRS alignments relative to the Hayabusa spacecraft, to AMICA, and to the wide-angle optical navigation camera (ONC-W) used for determination of the spacecraft position relative to the asteroid (2), were determined from in-flight star field calibrations. The coalignment between

the LIDAR and NIRS was confirmed when NIRS detected the reflected 1064-nm yttrium-aluminum-garnet–Nd (YAG–Nd) laser light from LIDAR (Fig. 1) and when changes in LIDAR ranges were found to correspond with expected changes in topography seen in AMICA data.

To measure the mass of Itokawa and its surface topography, the position of the Hayabusa spacecraft relative to Itokawa must be determined. We developed a new method (Fig. 2) to estimate this spacecraft position by combining a shape model (5) of the asteroid determined primarily from images, ONC-W information on the direction to the center-of-light from the asteroid, and LIDAR ranging data. With these data, a first guess at the spacecraft trajectory is made. Often, substantial discontinuities are observed that cannot be explained by thrusting. By least-squares fitting of a smooth function to the initial spacecraft trajectory, a more realistic smooth approximation is obtained, from which a cloud of LIDAR points sitting on the Itokawa surface can be determined. Checks with the actual location of the LIDAR spot in simultaneous AMICA images show that this method provides accurate spacecraft locations as well as good surface topography.

An example of the detailed surface topography that can be obtained from the LIDAR using this methodology is shown (Fig. 3) for data obtained from ~ 7 -km range. In this Tsukuba area (5), located on the eastern side of Itokawa and representative of the rough regions on the asteroid, blocks from 3- to 10-m elevation are visible. These data contrast significantly with results obtained

¹Graduate School of Science and Technology, Kobe University, Nada, Kobe 657-8501, Japan. ²Johns Hopkins University Applied Physics Laboratory, Laurel, MD 20723–6099, USA. ³Department of Computer Software, University of Aizu, Aizuwakamatsu, Fukushima 965-8580, Japan. ⁴Jet Propulsion Laboratory, California Institute of Technology, Pasadena, CA 91109, USA. ⁵Institute of Space and Astronautical Science (ISAS), Japan Aerospace Exploration Agency (JAXA), Yoshinodai, Sagami-hara, Kanagawa 229-8510, Japan. ⁶NEC Aerospace Systems Co. Ltd., Fuchu, Tokyo 181-8551, Japan. ⁷National Institute of Advanced Industrial Science and Technology, Tsukuba 305-8568, Japan. ⁸Department of Aerospace Engineering, University of Michigan, Ann Arbor, MI 48109–2140, USA.

*To whom correspondence should be addressed. E-mail: avell@kobe-u.ac.jp

from the Muses Sea, which is representative of smooth regions on Itokawa (6) where small-scale fluctuations in the elevation are observed that are comparable to the digitization of the LIDAR.

From such topographic data, the fractal roughness of the surface can be measured (7, 8) as the root mean square deviation σ of the height differences along a given baseline. For a 20-m baseline, which exceeds the LIDAR footprint, the Tsukuba region is characterized by a σ value of 2.2 m. This is in contrast to Muses Sea, where σ equals 0.6 m. Comparison of σ on Itokawa and Eros indicates that the rough Tsukuba region of Itokawa has a roughness on 20-m baselines similar to that measured in the interior, near the rim, of the large crater Psyche on Eros (8). This region in Psyche primarily consists of disrupted materials, strewn boulders, and coarse talus typ-

ical of crater ejecta. The similarity in roughness suggests that the near-surface of Itokawa resembles a rubble pile, which AMICA confirms (1, 6). To investigate the interior structure of Itokawa, we also measured the mass of Itokawa to determine its density. We used the best data available to us that the LIDAR acquired during the rehearsal descent phase on November 11, 2005.

The Hayabusa was designed as a simple spacecraft, with fixed antennas on the upper panel perpendicular to the +Z direction and fixed instruments on the base panel faced toward the -Z direction (toward the asteroid during in situ observations). On November 11, 2005, the Hayabusa spacecraft made a descent for the asteroid Itokawa along an Earth-Hayabusa-Itokawa line so as to allow both high-rate communication with Earth and in situ

observations of the asteroid. The solar phase angle, defined as a Sun-Itokawa-Hayabusa angle, was about 8° during the descent.

We estimated the acceleration term F of the spacecraft motion by using the descent data from 17:51:17 to 19:35:49 UT on November 11 (Fig. 4A) at distances from the center of Itokawa from 1427 to 825 m. We subtracted the effects of solar radiation pressure and thruster forces from the acceleration to estimate asteroid gravity. The thruster forces depend on injector temperature, and this contribution is presented as a function of thruster-injection rate when the maneuver uses only $\pm Z$ thrusters. The following relationship was derived from maneuver data obtained in mid-October about 10 km from Itokawa: F_{10} (cm/s^2) = $0.1603 \times (\text{thruster ratio}) + 1.5695 \times 10^{-5}$, where thruster ratio is defined as a ratio of an integrated time of thruster burn to the total time of interest, and the acceleration due to solar radiation is calculated as $1.3303 \times 10^{-5} \text{ cm/s}^2$.

During the above period of the descent, the thrusters were operated in only $\pm Z$ directions with a constant temperature of 35°C , and the total number of thruster injections was 136. Because the duration time of each thruster is 19.53 msec, the thruster ratio becomes 4.2348×10^{-4} , and the resulting F_{10} value is $8.3594 \times 10^{-5} \text{ cm/s}^2$. We assumed that the acceleration caused by solar radiation force and thruster effect is constant during the descent. As an initial condition, we subtract the above F_{10} value from the total acceleration term. Then, to investigate the gravity potential, we adopted a polyhedron method that was well suited to evaluate the gravitational field of an irregularly shaped body such as Itokawa (9), where we assumed a constant-density interior of the asteroid.

By least-squares fitting of the spacecraft orbit during descent to calculated orbits obtained with the Itokawa's polyhedron model, we estimate the gravitational potential GM of

Fig. 1. LIDAR spectrum observed by NIRS. The 0.1° by 0.1° square-shaped field of view of NIRS was coaligned with that of LIDAR (a 0.04° by 0.097° ellipse). LIDAR spectra reflected by Itokawa were detected by NIRS during the descent. Figure shows a LIDAR spectrum obtained by NIRS from an altitude of 900 m at 01:02:22 UT on November 12, 2005. Dotted line indicates observed LIDAR spectrum after subtracting a spectrum of the asteroid Itokawa. A preflight spectrum of LIDAR measured by NIRS is shown as a solid line for comparison with the one measured in flight. NIRS has a 64-channel InGaAs photodiode array detector corresponding to 764 to 2248 nm, which includes the reflected 1064 nm YAG-Nd laser light from LIDAR. The LIDAR signal detected by NIRS confirmed that LIDAR and NIRS instruments were coaligned within the field of view accuracy, i.e., 1.7 m at a distance of 1 km.

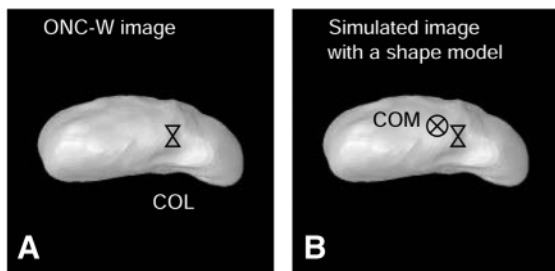
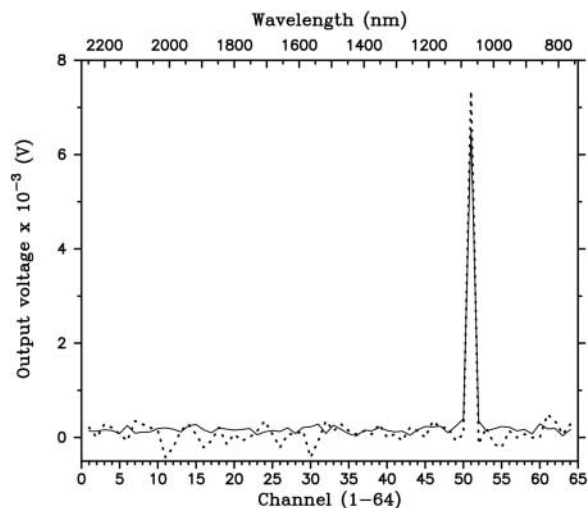
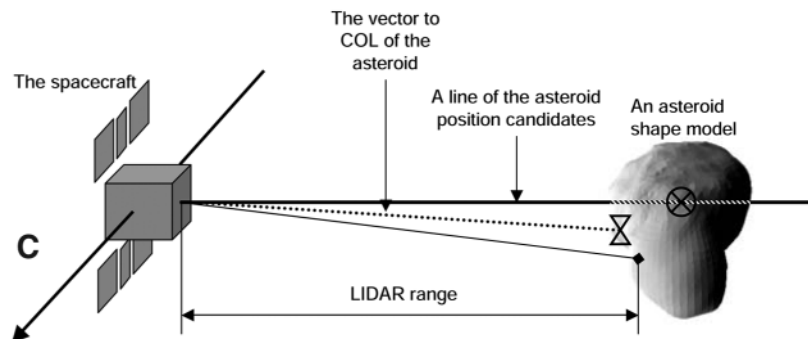


Fig. 2. Conceptual drawings of the method to estimate the position of the spacecraft. (A) ONC-W takes images of the asteroid every 128 s, and the onboard computer calculates the center of light (COL) of the asteroid image. The pixel coordination of COL in the camera detector is included in the telemetry. (B) With a shape model of the asteroid determined primarily from images (although any approximate shape model can be used), an artificial camera image of the asteroid is simulated. Even though this image is nonscaled, two vectors from the spacecraft to the COL and to the shape/mass center (COM) of the asteroid are obtained. (C) From COM



information and the simulated image, the location of the asteroid relative to the spacecraft is estimated with one degree of freedom on a line along the spacecraft-COM vector. Finally, the distance to the asteroid is obtained from an actual ranging data of LIDAR and the shape model. Through iterations, a very accurate spacecraft location can be found. This procedure was carried out on all pairs of the LIDAR ranging data and COL telemetry.

HAYABUSA AT ASTEROID ITOKAWA

Itokawa, where G is the gravitational constant and M denotes the mass of the asteroid (Fig. 4B). The resulting value of GM leads to the gravitational acceleration at a 10-km altitude, which is then also subtracted from the initial F_{10} to obtain an improved estimate of the solar radiation and thruster force. We then iterated the trajectory fit to the descent data to derive a revised value of GM using the modified F_{10} value and find a best estimate of GM equal to $(2.39 \pm 0.12) \times 10^{-9} \text{ km}^3/\text{s}^2$. The gravitational acceleration at the distance of 10 km from Itokawa is $\sim 0.2392 \times 10^{-5} \text{ cm/s}^2$, and it is about 3% of the acceleration term there.

Our GM value finds the mass of Itokawa to be $3.58 \times 10^{10} \text{ kg}$ with an uncertainty of 5%. The shape model of Itokawa constructed with AMICA images indicates that the volume is $1.84 \times 10^7 \text{ m}^3$ within 5% uncertainty (1). Consequently, the bulk density of asteroid Itokawa measures 1.95 g/cm^3 with 7% uncertainty. Our error in mass estimation is significantly larger than that obtained by the laser rangefinder aboard the Near Earth Asteroid Rendezvous mission (10), because Hayabusa did not orbit the asteroid, and the mass of Eros is 190,000 times that of Itokawa, producing greater uncertainty in the determination of spacecraft position.

Hayabusa NIRS reported that the Itokawa spectrum near the 1- μm absorption band is similar to those of LL-type chondrites (11). Considering the bulk density of LL ordinary chondrites of 3.19 g/cm^3 (12), our bulk density of asteroid Itokawa indicates a high porosity of about 40%, similar to that found for freshly formed coarse angular sands. Such a high porosity of Itokawa is noted in (1). It is known that the porosity of five S-type asteroids studied to date does not exceed about 20% (12), whereas two M-type asteroids have larger porosity of about 70%, and the average porosity of four C-type asteroids is about 28%. Our porosity for Itokawa is consistent with identification as a

Fig. 3. Location and elevation of LIDAR spot near Tsukuba region. (A) AMICA image ST2420994934 showing 17 predicted locations of LIDAR spot. (B) Simple cylindrical projection of the transect in meters North and East. (C) Relative elevation (m) along the LIDAR profile where the distance along the path is measured along the transect as if it were completely unwound. This elevation e is computed relative to a reference geoid as done in (7, 8): A ball would roll downhill from a high e to low e . The digitization error in these data are about $\pm 1.5 \text{ m}$. Data points in (B) are color coded by relative elevation according to (C). The letters in the lower two panels correspond to the circles seen in (A), going right to left. Panels (A) and (B) show how the location of the LIDAR spot fluctuates with time because of spacecraft pointing oscillations. Blocks with about 3- to 4-m elevation and the horizontal size of the order of the LIDAR spot are shown as sudden increases in elevation at locations D and G in (C). A jump at point J seen in elevation of about 5 m, and 10 to 15 m horizontally, corresponds to the central Tsukuba feature in (A).

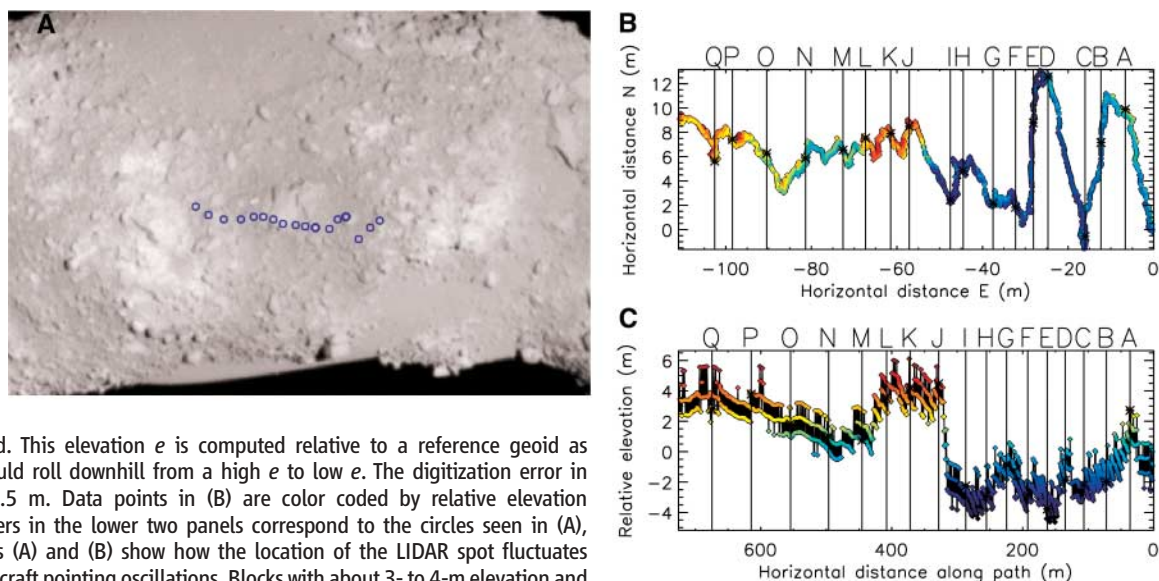
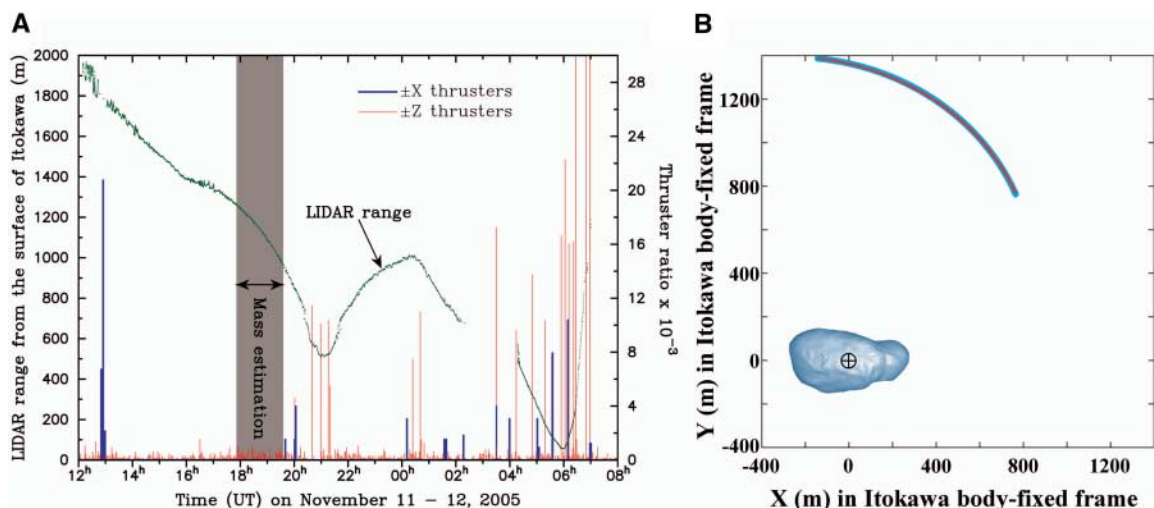


Fig. 4. (A) LIDAR range and thruster ratio during the rehearsal descent of November 11, 2005. LIDAR missed the surface during 2:20 to 4:17 UT. The period of 105 min for the mass estimation shows no abrupt changes and is very smooth relative to the other periods; moreover, the effect of thrusters in the direction of $\pm Z$ could be accurately estimated. (B) The position of Hayabusa in body-fixed frame (thick blue curve) was determined by LIDAR ranging data with images from the (ONC-W). This approach phase has a good opportunity to measure the gravitational field because the gravitational acceleration of Itokawa is about 18 times stronger than the acceleration as a result of solar radiation pressure at the distance of 1 km from



Itokawa. The red curve on the thick blue curve shows the computed trajectory of the Hayabusa spacecraft for the best fitted GM of $2.39 \times 10^{-9} \text{ km}^3/\text{s}^2$. The adopted shape model (5) for this computation is shown, with ellipsoidal diameters of 535 (X) by 294 (Y) by 209 (Z) m, respectively.

“loosely consolidated (rubble-pile) asteroid” (13). Itokawa is the first S-type asteroid showing such high porosity, and the first subkilometer-sized small asteroid showing a rubble-pile structure rather than a solid monolithic structure.

Two distinct types of terrain are found on Itokawa, rough terrain with numerous boulders and smooth terrain covered with regolith layer (6), which suggests a complex history but does not predicate a heterogeneous composition. In addition, no clear regional difference in the normalized x-ray intensity ratios of Mg/Si and Al/Si has been found on the surface of asteroid Itokawa (14), indicating homogeneous composition. NIRS reported olivine-rich mineral assemblages similar to LL5 and LL6 chondrites, with variations in albedo and absorption band depth more than 10%, but this diversity may be consistent with differences in freshness and/or particle size (11), and it does not suggest the presence of unusual inhomogeneous materials.

As noted in (15, 16), the size of the asteroid, 150 to 1000 m in radius, may be a transition size between monolithic structure and rubble-pile structure. The large porosity of ~40% and the roughness of the surface found on Itokawa strongly

suggest a rubble-pile structure. The 12.1324-hour spin period of Itokawa (I) is far above the critical value of 2 hours, where a rubble-pile structure cannot withstand centrifugal forces [e.g., (17)], and is also consistent with a rubble-pile structure.

The internal structure of the asteroid Itokawa gives us a hint of its origin. It is predicted, on the basis of the numerical simulation of orbital evolution of asteroid Itokawa, that the most probable source region of asteroid Itokawa is the inner part of the main belt (18). High porosity in asteroid Itokawa may be the result of gravitational aggregation of the collision fragments.

References and Notes

1. A. Fujiwara *et al.*, *Science* **312**, 1330 (2006).
2. T. Hashimoto, T. Kubota, T. Mizuno, *Acta Astronaut.* **52**, 381 (2003).
3. T. Mukai *et al.*, *Adv. Space Res.* **29**, 1231 (2002).
4. T. Mukai, A. M. Nakamura, T. Sakai, *Adv. Space Res.* **37**, 138 (2006).
5. H. Demura *et al.*, *Science* **312**, 1347 (2006).
6. J. Saito *et al.*, *Science* **312**, 1341 (2006).
7. A. F. Cheng *et al.*, *Science* **292**, 488 (2001).
8. A. F. Cheng *et al.*, *Icarus* **155**, 51 (2002).
9. R. A. Werner, D. J. Scheeres, *Celest. Mech. Dyn. Astron.* **65**, 313 (1997).
10. M. T. Zuber *et al.*, *Science* **289**, 2097 (2000).
11. M. Abe *et al.*, *Science* **312**, 1334 (2006).

12. D. T. Britt, D. Yeomans, K. Housen, G. Consolmagno, in *Asteroids III*, W. F. Bottke, P. Paolicchi, R. P. Binzel, A. Cellino, Eds. (Univ. Arizona Press, Tucson, AZ, 2002), pp. 485–500.
13. D. C. Richardson, Z. M. Leinhardt, H. J. Melosh, W. F. Bottke Jr., E. Asphaug, in *Asteroids III*, W. F. Bottke, P. Paolicchi, R. P. Binzel, A. Cellino, Eds. (Univ. Arizona Press, Tucson, AZ, 2002), pp. 501–515.
14. T. Okada *et al.*, *Science* **312**, 1338 (2006).
15. W. Benz, E. Asphaug, *Icarus* **142**, 5 (1999).
16. E. Asphaug, E. V. Ryan, M. T. Zuber, in *Asteroids III*, W. F. Bottke, P. Paolicchi, R. P. Binzel, A. Cellino, Eds. (Univ. Arizona Press, Tucson, AZ, 2002), pp. 463–484.
17. P. Pravec, A. W. Harris, T. Michalowski, in *Asteroids III*, W. F. Bottke, P. Paolicchi, R. P. Binzel, A. Cellino, Eds. (Univ. Arizona Press, Tucson, AZ, 2002), pp. 113–122.
18. P. Michel, M. Yoshikawa, *Astron. Astrophys.* **449**, 817 (2006).
19. Supported by ISAS/JAXA through the Hayabusa mission. We are extremely grateful for the numerous engineers and supporting scientists who were critical to the successful development and execution of the first mission that rendezvoused with and landed on an asteroid. We thank E. Okumura and K. Tsuno (NEC Toshiba Space Systems, Ltd.) for their great efforts to develop the LIDAR. This work is partly supported by the 21st Century COE Program “Origin and Evolution of Planetary Systems” under the Ministry of Education, Culture, Sports, Science, and Technology (MEXT).

15 February 2006; accepted 21 April 2006
10.1126/science.1126272

REPORT

Pole and Global Shape of 25143 Itokawa

Hirohide Demura,¹ Shingo Kobayashi,¹ Etsuko Nemoto,¹ Naoya Matsumoto,¹ Motohiro Furuya,¹ Akira Yukishita,¹ Noboru Muranaka,² Hideo Morita,³ Ken Shirakawa,³ Makoto Maruya,⁴ Hiroshi Ohyama,⁴ Masashi Uo,⁴ Takashi Kubota,⁵ Tatsuaki Hashimoto,⁵ Jun'ichiro Kawaguchi,⁵ Akira Fujiwara,⁵ Jun Saito,⁵ Sho Sasaki,⁶ Hideaki Miyamoto,^{7,8} Naru Hirata^{1,9}

The locations of the pole and rotation axis of asteroid 25143 Itokawa were derived from Asteroid Multiband Imaging Camera data on the Hayabusa spacecraft. The retrograde pole orientation had a right ascension of 90.53° and a declination of –66.30° (52000 equinox) or equivalently 128.5° and –89.66° in ecliptic coordinates with a 3.9° margin of error. The surface area is 0.393 square kilometers, the volume is 0.018378 cubic kilometers with a 5% margin of error, and the three axis lengths are 535 meters by 298 meters by 244 meters. The global Itokawa revealed a boomerang-shaped appearance composed of two distinct parts with partly faceted regions and a constricted ring structure.

A telescopic camera on Hayabusa, the Asteroid Multiband Imaging Camera (AMICA) (1), provided about 1400 pictures of Itokawa during its rendezvous phase (2). Members from the AMICA science team and the Guidance and Navigation Control (GNC) team formed a special task force to investigate Itokawa's shape and properties, based on images from AMICA. The task force derived the pole orientation and rotation axis and then formed a global shape model of Itokawa based on a subset of AMICA images. At the beginning of the rendezvous phase, Itokawa was scanned circularly by AMICA. This generated side views, whose mean

interval was about 2°, as well as two polar views. The total number of images was 212, and their resolution ranged from 0.7 to 0.3 m per pixel.

Itokawa's pole orientation was determined by optically tracking feature points, called ground control points (GCPs). The final pole orientation showed retrograde behavior; a right ascension of 90.53° and a celestial declination of –66.30°, or ecliptically as 128.5° and –89.66° with a 3.9° margin of error. The latest ground-based results confirmed the retrograde behavior of Itokawa and its rotation axis, which is almost perpendicular to the ecliptic plane (3–5). Because Itokawa's rotation axis is perpendicular to the ecliptic plane,

AMICA enabled global coverage without polar night regions during a rendezvous that lasted less than half of the orbital time of Itokawa. The north direction (+z) of Itokawa was defined by the International Astronomical Union's right-hand-rule of its own rotation (6), and the +z axis was set to the minimum principal axis of inertia. The direction of the prime meridian (+x) was defined by a GCP, the Black Boulder. The rest of the +y was fixed. This coordinate system was rotated 180° around the z axis with that of previous shape models (4, 7, 8).

The global shape of Itokawa was reconstructed with image-based modeling that integrated limb profiles and stereogrammetric procedures (9). The total number of automatically selected feature points for three-dimensional shape modeling was 308,205, which were related to boulders rather than small distinct craters. Spacing of the points was not ordered, and smooth terrains revealed an absence of such

¹Department of Computer Software, University of Aizu, Ikki-machi, Aizu-Wakamatsu City, Fukushima 965-8580, Japan. ²CosmoLogic, 3-5-7, Kirigaoka, Midori-ku, Yokohama 226-0016 Japan. ³NEC Aerospace Systems, 1-10 Nissincho, Fuchu, Tokyo, 183-8551 Japan. ⁴NEC-TOSHIBA Space Systems, 1-10 Nissincho, Fuchu, Tokyo, 183-8551 Japan. ⁵Institute of Space and Astronautical Science/Japan Aerospace Exploration Agency, 3-1-1, Yoshinodai, Sagami-hara, 229-8510 Japan. ⁶National Astronomical Observatory of Japan, 2-12 Hoshigaoka, Mizusawa, Oshu 023-0861, Japan. ⁷Department of Geosystem Engineering, University of Tokyo, Tokyo 113-8656, Japan. ⁸Planetary Science Institute, 1700E Fort Lowell, Suite 106, Tucson, AZ 85719, USA. ⁹Graduate School of Science and Technology, Kobe University, Kobe 657-8501, Japan.